MJSAT

Malaysian Journal of Science and Advanced Technology

journal homepage: https://mjsat.com.my/

Interpretation of Aeromagnetic Anomalies and Structural Framework Over the Southern Part of Sokoto Basin, NW, Nigeria, Using Digital filtering Tools

Abubakar Adamu*[1], Kasimu Kuka Shehu[1], Alhasan Sadiq Abubakar[1], Abdulrahman Augie Idris[1], Mubarak Fana Muhammad[1], Hadiza Tsafe Umar[1], Sufyan Umar[1], Aliyu Kaura Mohammed[2], Kelvins Godfrey Ugbena[3], and Abdulrahman Olatunde[4]

[1]*Federal University Birnin Kebbi, P.M.B 1157, Nigeria.*
[2]*Federal University of Lafia, Nasarawa, P.M.B 146, Nigeria.*
[3]*Prince Abubakar Audu University Anyigba, Kogi State, Nigeria.*
[4]*Science Laboratory Technology, Federal Polytechnic Bauchi, P.M.B 1058, Nigeria.*

KEYWORDS

Aeromagnetic anomalies
Tectonic trends
Digital filtering tools
Metalliferous minerals
Sokoto Basin

ARTICLE HISTORY

Received 8 February 2024
Received in revised form 30 May 2024
Accepted 22 June 2024
Available online 11 July 2024

ABSTRACT

The Taloka formation Sokoto Basin, Nigeria, was studied in an effort to discover and map the structural features favourable for metalliferous mineral deposits. High-resolution aeromagnetic data was subjected to structural analysis in order to map and highlight structural lineaments and their trends, as well as the depth of magnetic source bodies. Several digital filtering approaches were used to analyze, process, and interpret the data, including total gradient, total horizontal derivative of tilt of angle derivative (THDR_TDR), source parameter imaging (SPI), and spectral depth analysis. The RTE method was employed to prevent the North-South signal from predominating the results because the area was within the low latitude zones. The eastern Gundumi formation (Marafaro, Rujin Tsamia, Kwanawa, Dande, and Rikaka), the northeastern Taloka formation (Dutsen Bature, Bange, and Kumazo), and the western Taloka formation (Bejiji, Bagu, Danjiru, Baranzaki, and Awakala) are all found to have low amplitude magnetic anomalies. The research area exhibits magnetic anomalies with strong amplitudes (0.078 nT/m), which are consistent with the total gradient (AS) approach and might be caused by ferromagnetic minerals like iron stone. The aforementioned filters were also used to outline the lineaments (such as faults, fractures, or shear zones) believed to be associated with alteration zones, which are essential in locating the mineralized zones. The lineaments typically trend in the E-W, NW-SE, and NE-SW directions. Utilizing the SPI techniques, the depth of occurrence of the causative bodies was found to be below 250.3 m. The crustal magnetic field values were utilized to generate the two-dimensional Fourier transforms, from which the radial spectrum was recovered. The depth values were calculated using the slopes of the sixteen sections' spectrum energy against frequency graph. According to the findings, the study area's deeper depth lies between 1.10 and 1.69 km, while its shallower depth lies between 0.39 and 0.90 km. The study finds that alteration zones may harbour minerals and that the thickness of the sedimentary layer may not be sufficiently buoyant to support the build-up of hydrocarbons but will enhance the possibility of other mineralization.

1. INTRODUCTION

Several rift-related basins, including the Sokoto Basin, have important geological and structural features that could be visible at the surface or hidden beneath the surface. Seismic, gravity, and/or magnetic methods are frequently used by researchers to evaluate the structural and tectonic framework [1] and [2]. High resolution aeromagnetic (HRAM) datasets have produced accurate and reliable surface and subsurface basin results when seismic datasets are not available. Uncertainty in exploration can be decreased by developing new workflows and procedures and refining the way

*Corresponding author:
E-mail address: Adamu Abubakar <adamu.abubakar35@fubk.edu.ng>.
https://doi.org/10.56532/mjsat.v4i3.261

aeromagnetic data is processed. Recent improvements in the processing of aeromagnetic data have made it possible to significantly reduce exploration uncertainty. In inland basins (like the Sokoto basin), where folding and faulting may have resulted in the development of complex structural geometry, the identification of anomaly source is even more challenging.

In general, variations in the earth's magnetic field are depicted in aeromagnetic maps as the magnetic properties of the underlying rocks, such as their magnetic susceptibilities. Sedimentary rocks have the highest magnetic susceptibility [3] and the lowest magnetic susceptibility compared to metamorphic, acidic, intermediate, and basic igneous rocks. The basement level of crystalline (igneous or metamorphic) rocks is hence where a magnetic signal or anomaly is produced in the highest quantity [4]. Magnetic anomalies over sedimentary terrain are often brought on by the basement rocks beneath, which may be igneous and/or metamorphic, or by igneous structures such as intrusive plugs, dykes, sills, lava flows, and volcanic centers. Rocks that contain magnetic minerals are what generate magnetic anomalies. High sensitivity readings, however, may also be related to anthropogenic changes in sedimentary rocks and cultural iron contamination [5] [6], possibly brought on by hydrocarbon migration.

This study's major aim was to analyze and interpret HRAM data over the Taloka formation and its surroundings. The study's three major objectives were to map out the locations of deposits of metalliferous minerals, identify structural trends and lineaments, and calculate the depth of magnetic source bodies in the area's sedimentary layer. Such structural lineaments include veins, shear zones, fractures, and faults, which frequently operate as possible hosts or migration routes for groundwater, hydrocarbons, and minerals. Sediment thickness in any sedimentary basin is essential for the production of fossil fuels.

In Taloka and the surrounding areas, the study revealed the significance of aeromagnetic data for mapping metalliferous mineral deposits, especially iron ore with a high magnetite-to-haematite ratio, establishing structural lineaments, and determining sedimentary cover (sediment thickness). In order to understand the structural patterns of crustal expansion over the Sokoto basin using HRAM data in the temporal and frequency domains, it is important to re-evaluate the magnetic anomaly of these border locations.

2. STUDY AREA: LOCATION AND GEOLOGICAL SETTING

2.1 Location of the study area

The study region is located in the southern part of the Sokoto basin (Rabah), in Northwestern Nigeria. Its limits are defined by longitudes 5° 00' E and 5°30' E, as well as latitudes 13° 00' N and 13°30' N. In the sub-Saharan Sudan region of West Africa, the Sokoto basin in Northwestern Nigeria is surrounded by vegetation resembling a savannah. With an average annual rainfall of about 30 inches, the rainy season, which lasts from May to October, brings rainfall to the bulk of the basin. The long dry season, which lasts from October to April, is characterized by dusty harmattan gusts from the northeast. April and May are the hottest months, with occasional readings of 105 °F.

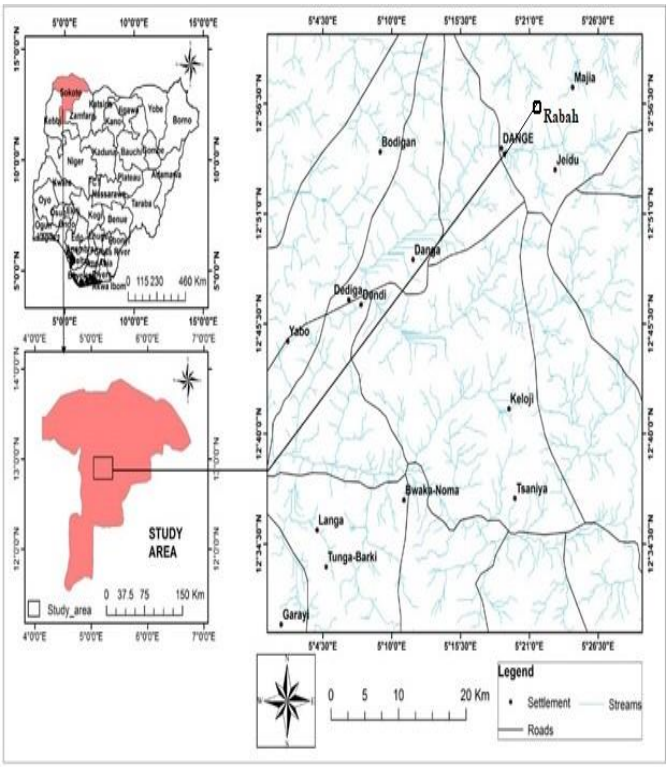

Fig. 1. Map showing the location of the study area (modified from Arch-GIS, 2019)

2.2 The Geological settings

The Sokoto Basin is a depression of the Iullemmeden Basin, which covers a total area of around 700,000 km^2 and is located in the northwest of Nigeria and the southeastern section of the Iullemmeden Basin [7]. One of the more recent cratonic sedimentary basins in West Africa that dates from the Tertiary to the Mesozoic is the Sokoto Basin. The basin originated through epierogenetic warping, stretching, and rifting of the crust, similar to other transcontinental basins in the area and the African continent in general. Four depositional periods resulted in the accumulation of sediments in the Iullemmeden Basin [2]. The Gundumi Formation, which is made up of adits and clays that make up the Premastrite Continental Intercalaire of West Africa, lies above the nonconforming Precambrian basement. The masstritichtian Rima group uneasily encroaches upon them. Fossiliferous, calcareous, and Shaley Dukamaje Formations divide the mudstone and sandstone of Taloka and Wurno Formations from one another. The calcareous Kalambaina Formation divides the shale-dominated Dange and Gamba Formations, which make up the Paleocene Sokoto Group. The Gwandu Formation, which is situated above the continental crust, is composed of the post-Paleocene continental terminal. These sediments gradually thicken and softly deepen as you approach toward the northwest.

3. METHODOLOGY

According to [8] [9] [10] the magnetics technique identifies the sub-surface spatial distribution of rock magnetization characteristics, J, or susceptibility, k, and remanence, which results in changes in the Earth's magnetic (geomagnetic) field intensity and direction.

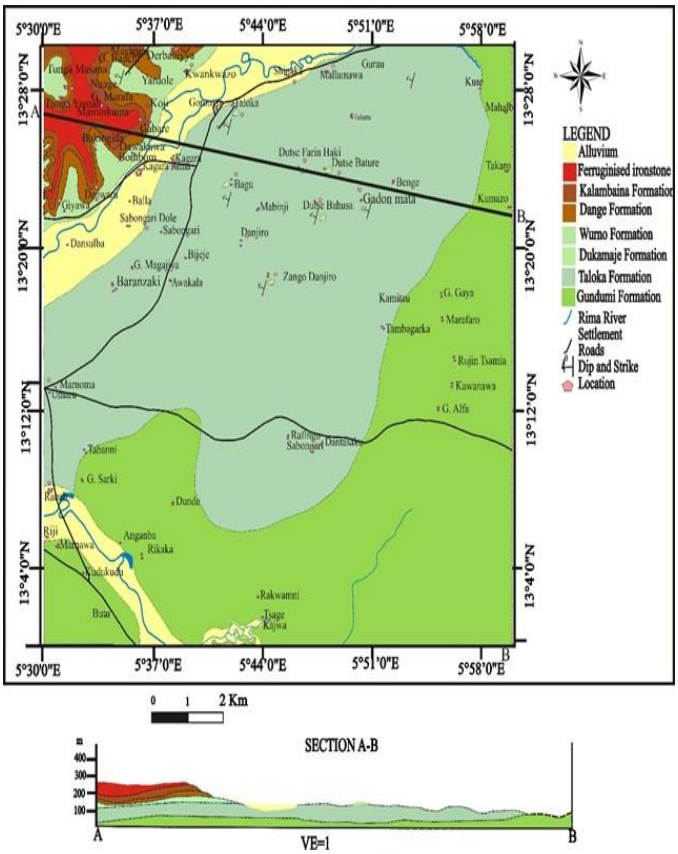

Fig. 2. Map of the study area's geology modified after [2]

The geomagnetic field is a geographical region of space under the control of the magnetic field of the Earth's nucleus [10]. It is made up of the three major sources listed below.

$$B_{obs} = B_{core} + B_{crust} + B_{external} \quad (1)$$

In this model, B_{obs} is the observed geomagnetic field, B_{core} is the magnetic field derived from the core, B_{crust} is the local anomaly of the magnetic field caused by the presence of unusual crustal and/or heliospheric magnetic sources, and $B_{external}$ are the ionosphere, magnetosphere, and atmosphere contribution, which is typically regarded as very noisy in studies of the crust or core.

The core field of the planet B_{core} described for a period of five years using the IGRF, a widely used mathematical model [9]. Earth-based magnetic field information, or B_{crust}, is data that has been collected from ships, planes, or the ground. These come from the magnetization of crustal rocks that include ferromagnetic minerals such magnetite, titanomagnetite, and pyrrhotite at temperatures below the Curie point [10] [11]. Furthermore, it's crucial to keep in mind that induced magnetization—a type of magnetization that is caused by an external magnetic field—can occur. The Earth's magnetosphere and ionosphere can both contribute to the geomagnetic field in external ways. In marine and aeromagnetic data sets, the $B_{external}$ adds short wavelength noise [12] [8]. To produce crustal magnetic anomalies, integrated models must be subtracted by the full long wavelength caused by core magnetic fields as well as exterior fields from magnetic field data. A variety of components can be split into when measuring the geomagnetic dipole field (Fig. 3). According to [12] [8], In contrast to declination, which is the angle created on a horizontal plane by true north and magnetic north, magnetic inclination, or I, is the angle produced by the magnetic field vector and the plane.

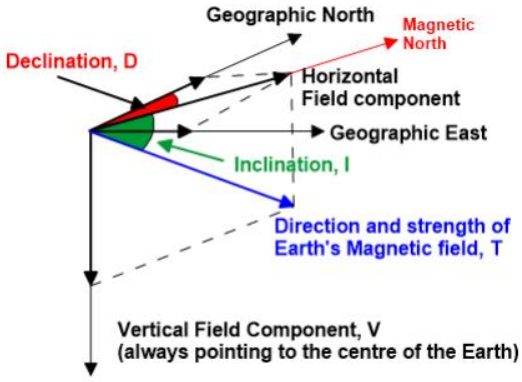

Fig. 3. Elements of the measured geomagnetic field

According to [13], the magnitude or strength (TMI or T) of the magnetic field, which stands for local magnetic field anomalies superimposed on Bobs where crustal materials carrying magnetite are found, is related to Bobs in equation 1. While T is easily measured by magnetometers and represents the strength of the magnetic fields produced in response to the macroscopic magnetization currents on the surface of anomalous magnetic media in the subsurface, Bobs is the total magnetic response of the microscopic and macroscopic surface magnetization currents [13].

$$T_{obs} = T_{core} + T_{crust} + T_{external} \quad (2)$$

The measured T is represented by T_{obs}, the core-derived field is represented by T_{core}, the local variations of T caused by the presence of anomalous crustal magnetic sources are represented by T_{crust}, and the air contributions (Noise) are represented by $T_{external}$, It is presumed that these variables are parallel. The discrepancy between the actual and theoretical TMI values for each location, assuming that external contributions have been eliminated, is known as the total magnetic field intensity (TMI) anomaly, or T.

$$\Delta T = T_{crust} = T_{obs} - (T_{core} + T_{external}) \quad (3)$$

The magnetization of T_{core} causes it to create secondary magnetic fields, or T, in crustal magnetic minerals. Induced magnetization (J_i) and remanent magnetization(J_v) are added to determine the volume of the crustal magnetization (J_v), (J_i) refers to the magnetization that is seen in rocks that include ferrimagnetic minerals when inducing or ambient magnetic fields are present, whereas J_r refers to the magnetization that is seen in ferrimagnetic materials when there is a permanent record of magnetizations that a rock has accumulated over its history [11].

$$J_v = J_i + J_r \quad (4)$$

Where J_v = kT and k is the magnetic susceptibility, a dimensionless constant that is positive when the Jr is pointing in the same direction as J.

3.1 Materials

In this study, high-resolution aeromagnetic data from Sheet 10 of the Geological Survey of Nigeria was employed, which was generated at a scale of 1:100,000. The HRAM data were collected across a sequence of NW-SE flight lines that were separated by 20 km between tie-lines, 2 km between flight lines, and 500 feet (152 m) of theoretical flying altitude. A Scintrex CS3 cesium vapour magnetometer sensor was mounted on the fixed wing of the aircraft and utilized to record the magnetic datasets. The collected grid data was combined and assembled to produce the composite map of the study region. The composite map of the study area was created by combining and assembling acquired grid data. By merging and putting together the gathered grid data, the composite map of the research region was produced. The coordinate systems X (longitude measured in meters), Y (latitude measured in meters), and Z (magnetic intensity measured in nano Tesla) were further converted into digital versions. The corrected aeromagnetic information was gridded with the minimal curvature method using Geosoft Oasis Montag v. 8.4 software to create a map of the total magnetic intensity (TMI) of the study area. To prevent aliasing problems, the map was digitalized at 1-kilometer intervals. The thinnest magnetic source body that could have been identified from the digitized data would have had a thickness of roughly 2 km broad since this time imposed a 12/km (i.e., 0.5/km) Nyquist wavenumber.

3.2 Reduction to equator of magnetic field (RTE)

According to [14], the RTE operator is typically used to find the center of magnetic anomalous lows over the disruptive source at low magnetic latitudes. The TMI's amplitude is adjusted by RTE, and N-S structures are suppressed. By eliminating the impacts of magnetic inclination and maintaining the amplitude of the anomaly, this technique creates a map that can be understood. Assuming that the source's entire magnetization is induced, the 2D FFT calculation for the RTE operator in the wavenumber domain yields the following expression:

$$(\boldsymbol{\theta}) = -\cos^{-}(\boldsymbol{D}+\boldsymbol{\theta})/[\sin(\boldsymbol{I})+\boldsymbol{i}\cos(\boldsymbol{I})\cos(\boldsymbol{D}-\boldsymbol{\theta})]^{2} \quad (5)$$

The horizontal wavenumber component direction, the square root of one, the magnetic field's inclination and declination, as well as the magnetization of the causative body, are represented by the letters, θ, i, I, and D, respectively. The amplitude component is known as sin (I), while the phase component is known as i cos (I) cos ($D - \theta$). In order to translate magnetic data, which is frequently expressed in the x and y directions in the space domain, into the wavenumber domain, the 2D FFT is used. As a result, the computation of the procedure is expedited [14]. The Fourier domain function is typically sampled in the wavenumber domain at even intervals between 0 and the Nyquist wavenumber (1/ [2*cell size]) of 1/ (grid size) (cycles/meter). As a result, the major representation is centered on zero, and the values closer to the center point are dominated by long wavelengths [8]. Wavenumbers typically have both negative (imaginary) and positive (actual) components.

3.3 Digital filtering tools used for data processing

The equations are an exception to the prescribed specifications of this template. You will need to determine whether or not your equation should be typed using either the Times New Roman or the Symbol font (please no other font). To create multileveled equations, it may be necessary to treat the equation as a graphic and insert it into the text after your paper is styled.

3.4 Digital filtering tools used for data processing

3.4.1 Total gradient approach for analytic signal

The analytical signal (AS), total gradient or analytic signal magnitude is expressed as the sum of the roots of the product of the vertical and horizontal derivatives of the magnetic and gravity fields. Maxima (ridges or peaks) of the analytical signal are seen directly above fault blocks or faults, lithological contacts, shear zones, volcanic plugs, dykes, etc., while some lie over the edges to help in detecting linear structures [15] [16] [17] [18]. Due to the employment of a constant-amplitude function, this derivative is usable at low magnetic latitudes [15] [19]. The AS can be noisy, especially at low magnetic latitudes where there may be a lot of anomaly distortion [20]. The AS is independent of the orientation of the magnetizing source.

$$\text{ASA} = \sqrt{(\frac{\partial T}{\partial x})^2 + (\frac{\partial T}{\partial y})^2 + (\frac{\partial T}{\partial z})^2} \quad (6)$$

T stands for the measured total magnetic field.

The $(\frac{\partial F}{\partial x})^2$, $(\frac{\partial F}{\partial y})^2$ and $(\frac{\partial F}{\partial z})^2$ are the squares of the x, y, z derivatives of the Magnetic anomaly [15].

3.4.2 Derivative method for total horizontal of tilt angle

The lateral extent of unusually dense or magnetic entities and their edges have been mapped using the tilt derivative [21] [22]. It differs slightly from the local phase in that the absolute value of the horizontal derivative, or local wavenumber, is utilized as the denominator. According to [22] [23], the combination of tilt derivative and total horizontal derivative generates sharp edges and is hence excellent for mapping shallow structures.

The tilt derivative was stated as follows by [22]:

$$\text{TDR} = \text{arc}tan^{-1}(\frac{VDR}{THDR\_TDR}) \quad (7)$$

Where the total horizontal and vertical first derivatives of gravity or total magnetic strength, respectively, are denoted by the letters VDR. While TDR_THD is provided as the tilt to the horizontal derivative.

$$\text{THDR} = \sqrt{\left(\frac{\partial T}{\partial x}\right)^2 + \left(\frac{\partial T}{\partial y}\right)^2} \quad (8)$$

TDR in equation 7 is the tilt.

The borders of lineaments can be identified by a plot of the zero of tilt [24] [25], and the slopes across the zero of tilt contour can be used to identify the throw direction of faults [22]. When the density or susceptibility contrasts are large, the tilt derivative approach is constrained; in other words, the anomaly will be large if the contrast is great and vice versa. The tilt derivative may not provide an adequate representation of magnetic structures at low latitudes due to the effects of the magnetic field's anisotropy, which results in structures having

a range of striking azimuths [22]. Although it is near the edge of the structure, the zero crossing of the tilt derivative has the benefit of levelling susceptibility and facilitating signal-to-noise separation.

3.4.3 Local wavenumber of the source parameter imaging

The tilt angle along a 2D profile, also known as the horizontal gradient of the local phase, is what is known as the local wavenumber [26] [27]. According to [28], it is used to determine the depths to the tops of buried bodies and often requires second-order derivatives of the gravity or total magnetic field. The maxima are stated to be superior to the analytical signal method for mapping geology and are found over single contacts. With maxima directly over the contacts, the local wavenumber peaks over linear features. It is derived from the first and second derivatives of the observed gravity or magnetic field. It is significantly impacted by noise. For a grid, the formula is stated as a more straightforward local wavenumber estimate [23] [29].

According to [28], an equal expression for the local wavenumber of the gridded anomalous magnetic field $M(x, y)$ is given by;

$$k(x,y) = \frac{1}{|A(x,y)|^2}\left(\frac{\partial^2 M}{\partial x \partial z}\frac{\partial M}{\partial z} + \frac{\partial^2 M}{\partial y \partial z}\frac{\partial M}{\partial y} + \frac{\partial^2 M}{\partial z^2}\frac{\partial M}{\partial z}\right) \quad (9)$$

For profile data, $|A(x,y)|^2$ is defined as;

$$|A(x,y)|^2 = \left(\frac{\partial M}{\partial x}\right)^2 + \left(\frac{\partial M}{\partial y}\right)^2 + \left(\frac{\partial M}{\partial z}\right)^2 \quad (10)$$

The expressions for the vertical and horizontal gradients of the sloping contact are [27]:

$$\frac{\partial T}{\partial z} = 2KFc \sin d \frac{x\cos(2I-d-90) - h\sin(2I-d-90)}{h^2+x^2} \quad (11)$$

$$\frac{\partial T}{\partial x} = 2KFc \sin d \frac{h\cos(2I-d-90) + x\sin(2I-d-90)}{h^2+x^2} \quad (12)$$

Where $K$is the susceptibility contrast at the contact, F is the magnitude of the Earth's magnetic field, $c = 1 - cos^2 i\ sin^2\alpha$, α is the angle between the positive x-axis and magnetic north, i is the ambient field inclination, $tan\ I = tan\ i/cos\ \alpha$, d is the dip (measured from positive x-axis), h is the depth to the top of the contact and all trigonometric arguments are in degrees. Where the coordinate system has been defined, such as x = 0 directly above the edge of the source. It is frequently demonstrated that the maxima of the local wave number are independent of the magnetization directions. Thus, the peaks outline the source edges at locations, $x = 0$.

3.4.4 Spectral depth analysis

The spectrum depth estimation methodology can be used to estimate the deep extent of magnetic sources by examining the statistically significant features of magnetic anomalies [30]. This method demonstrates the relationship between the spectrum of magnetic anomalies and the depth of a magnetic source by transforming the spatial data into the frequency domain. According to [31], this approach is more suitable for regional collections of magnetic abnormalities. [32] [31] state that the slope of the high wavenumber section of the power spectrum is used to compute the height of the magnetic source as follows:

$$\mathrm{Ln}\left(p(K)^{\frac{1}{2}}\right) = B - [K]Z_t \quad (13)$$

Where P(K), Z, and B are the depth to the top of the magnetic source, the power density spectrum, and the magnetic field constant, respectively. An estimate of the magnetic source's depth can be obtained from a power spectrum versus frequency diagram. Deeper sources are represented by the plot's low frequency part, while shallow sources and noise are represented by the plot's intermediate frequency and high frequency segments, respectively. Z = — $\frac{m}{2}$ for frequency units in radians per kilometer and Z = — $\frac{m}{4\pi}$ for frequency units in cycles per kilometer, where m is the slope, gives the mean depth, Z, to the magnetic source. For the purposes of this investigation, the Depth to magnetic source for each block was calculated using the formula - m/(4), and the results are shown in Table (1).

4. RESULTS AND DISCUSSIONS

4.1 The processing of magnetic datasets

The magnetic dataset used in this study was based on High-resolution aeromagnetic (HRAM) data which Fugro Airborne Surveys gathered for the Nigerian Geological Survey Agency (NGSA). Three Scintrex CS3 Cesium Vapour magnetometers were used in the survey, which was conducted along a sequence of flight lines that ran from northwest to southeast (135 degrees), perpendicular to the main regional geologic structural trend. Between 2005 and 2007, as part of the African project's first phase, this was accomplished using 500 m line spacing and a 5000 m tie-line spacing. The resolution was better than previously published high-altitude data [18] because the data were collected at 0.1-second intervals with an 80 m mean terrain clearance. The study region was covered by one aeromagnetic grid made up of five individual grids, each measuring roughly 10 km × 10 km (Fig. 4). A TMI map for the research area was created using a bi-directional gridding technique with cells that were 125 m by 125 m in size, or one-fourth the distance between flight lines [14] [23]. Anomalies on short, medium, and long wavelengths are what define the TMI, which has a range of -2330.6 nT to 1259.2 nT. Most often outside the basin and in a few locations inside the basin that are characterized by basement highs and intrusive rocks, the short wavelengths (high wavenumber) anomalies are seen. The deep magnetic anomalies linked to the deep basement are indicated by the long-wavelength (low wavenumber) abnormalities observed throughout the basin. In comparison to the similar work at high latitudes, interpreting TMI anomalies in low magnetic latitudes is very difficult [5]. Finding a method that will vertically align the magnetization direction and the measured field's direction is one of the challenges experienced at low magnetic latitudes. Without achieving this, the anomaly will be displaced laterally in relation to its source and have a twisted shape, making magnetic and geologic interpretations more challenging [11]. Over time, TMI anomalies have been transformed to align

over their sources using reduction to the equator or the pole procedures [5] [33], which help with geologic interpretation.

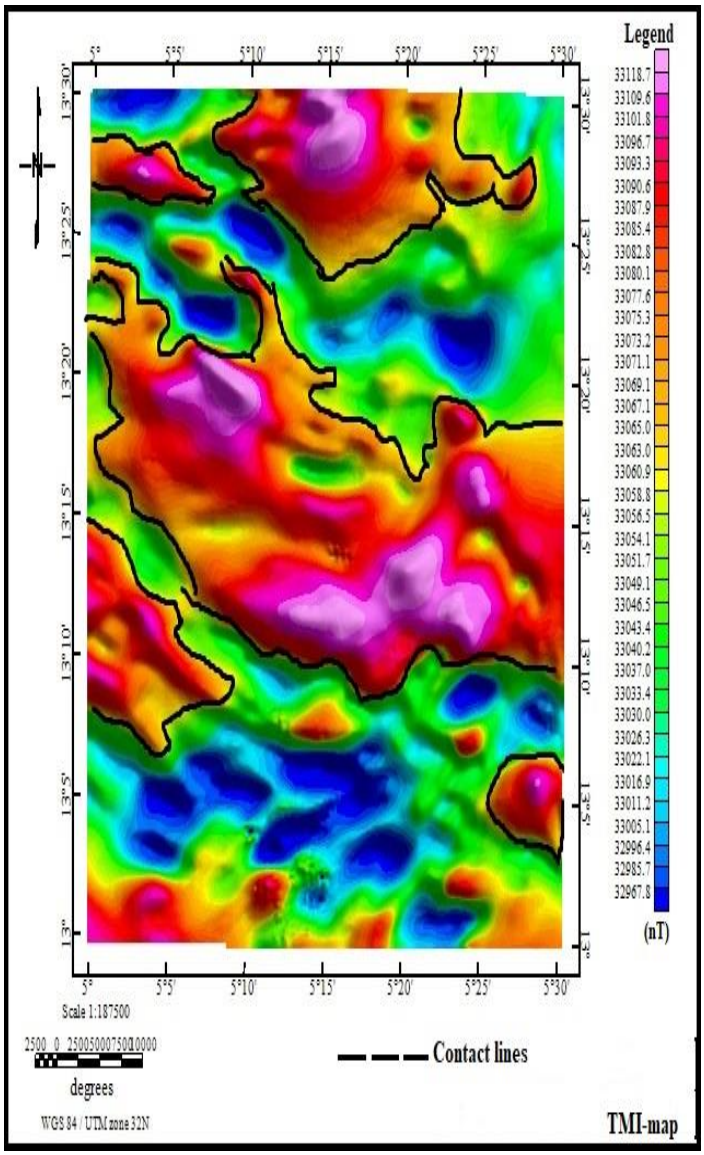

Fig. 4. Map of the total field intensity over the study area, the purple to red colours on the (TMI) indicate region with high magnetic values, while the blue colours denote areas with low magnetic values

4.2 Reduced to magnetic equator, RTE

Without significantly sacrificing any geophysical significance, the RTE transformation yields a result similar to the TMI. Both the RTE transform and the RTP, which become unstable at low geomagnetic latitude, assist in shifting anomalies over the source magnetizations [18]. The drawbacks of this method include the potential for unfavourable outcomes, such as the minor amplification and extension of abnormalities in East-West directions and the inability to image N-S features. Magnetic inclination and declination have an impact on how the RTE transformation behaves. According to the IGRF model, these characteristics exhibit substantial regional differences. Inclination varies from -4.37° in the north to -16.43° in the south, and declination falls from -1.07° in the north-eastern region to -2.88° in the south. These huge variances in the geomagnetic inclination and declination suggest that the RTE operator may provide unintended effects if average values are applied. Consequently, it might be best in this situation to differentially reduce the TMI. The use of this technique has been limited to regions with high geomagnetic latitudes and very strong magnetic inclinations and declinations [9]. In this study, a similar method known as the differential reduction to the equator methodology was adopted and used to the TMI data with the intention of limiting the impacts of the fluctuation in inclination and declination on the RTE results. In this study, a similar method known as the differential reduction to the equator methodology was adopted and used to the TMI data with the intention of limiting the impacts of the fluctuation in inclination and declination on the RTE results. The calculated mean inclinations and declinations from one of the strips were used to apply the standard RTE transform numerous times to the entire area. On first glance, the RTE map appears to be quite similar to the TMI map, however closer examination reveals that the RTE has assisted in locating the anomalies around unsettling sources (shown on the map as contact lines). Over sources of disturbance with negative magnetic susceptibility are directly located negative RTE magnetic anomalies.

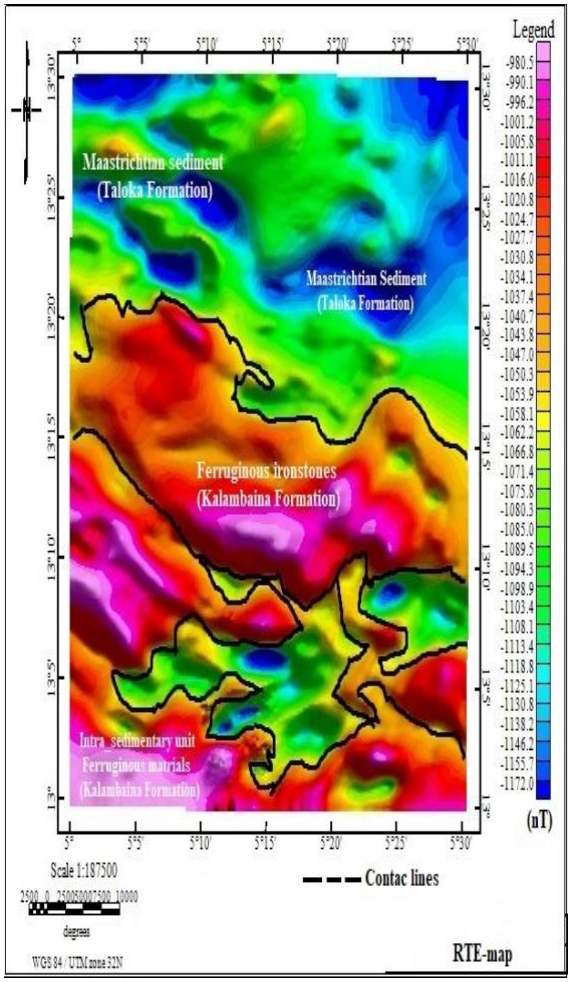

Fig. 5. Reduce to magnetic equator map of the Study area. Anomalies are displayed as vertically positioned; the black lines (contact) have undergone significant transformation

4.3 Total gradient (analytic signal)

This method was applied to the RTE grid map in order to identify the features of the earth's source materials as well as the precise locations of the causal body. The boundaries of the texture of the anomaly are also identified, as well as the change in the magnetization of the magnetic sources. In addition, the magnetization's orientation is discovered. From Figure 6, we can see that the amplitude was high (0.078 nT/m) over the edge of the magnetic structures in the NW part of the Kalambaina formation and southern part of the intra sedimentary unit (Sokoto group) due to magnetic anomalies around these areas, which are associated with ferromagnetic properties that are more of Fe-bearing rocks. When compared to the geology of the research area, these strong magnetic zones were associated with iron stone, hematite, magnetite, and siltstones. Ferromagnetic minerals, which often belong to the family of iron-rich minerals and include manganese ore, exhibit significant positive magnetic anomalies in these zones. The low magnetic zones, whose amplitudes range from 0.009 to 0.004 nT/m, are also identified as being located in the Taloka Formation's NE portion, as well as in the Illo and Gundumi Formation's eastern and western pre-maastrichtian deposits. When compared to a geologic map, these areas of low amplitude are related to sandstones, clays, shale, limestone, and laterites. In certain areas, diamagnetic minerals are present, which often have a weak negative magnetic anomaly within the sedimentary Basin.

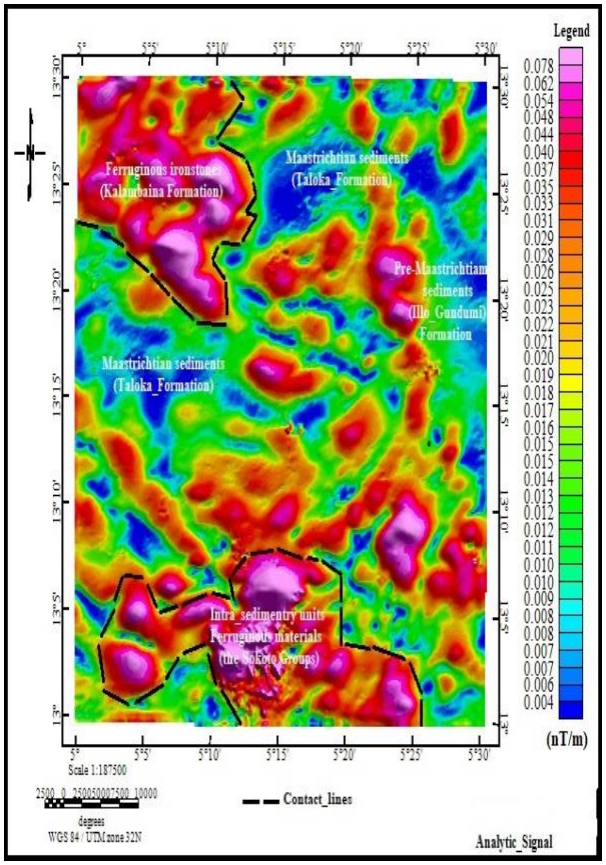

Fig. 6. The limits of the Cretaceous and Tertiary deposits are shown on a map of the study area's total gradient magnitude (analytic signal)

4.4 Total horizontal tilt angle derivative

The examination of the total horizontal and tilt angle derivatives, or THDR_TDR, reveals the magnetic lineaments that represent faults in the earth's crust. The horizontal position with edge extent is made easier with this technique. The location of abrupt changes in magnetic susceptibilities between positive and negative anomalies, particularly at the sharp gradient, is assumed to be the region on the TDR map where there are no magnetic anomalies. The contact boundary of magnetic sources is therefore the region with zero magnetic values. When looking at the colour scale bar in Figure 7, it is possible to identify the region of zero magnetic value as being light yellow. This region is located between the green (negative values) and red (positive values) colours.

The tilt derivative map (Fig. 7) highlights short spectral anomalies and is highly helpful in identifying shallow near-surface features and mineral exploration opportunities [5]. The map shows features (faults, fractures, and shear zones) in the northern, south-western, north-western, and south-eastern portions of the research region that may house solid minerals because minerals are structurally controlled by these structures, which trend NE-SW, NW-SE, and E-W.

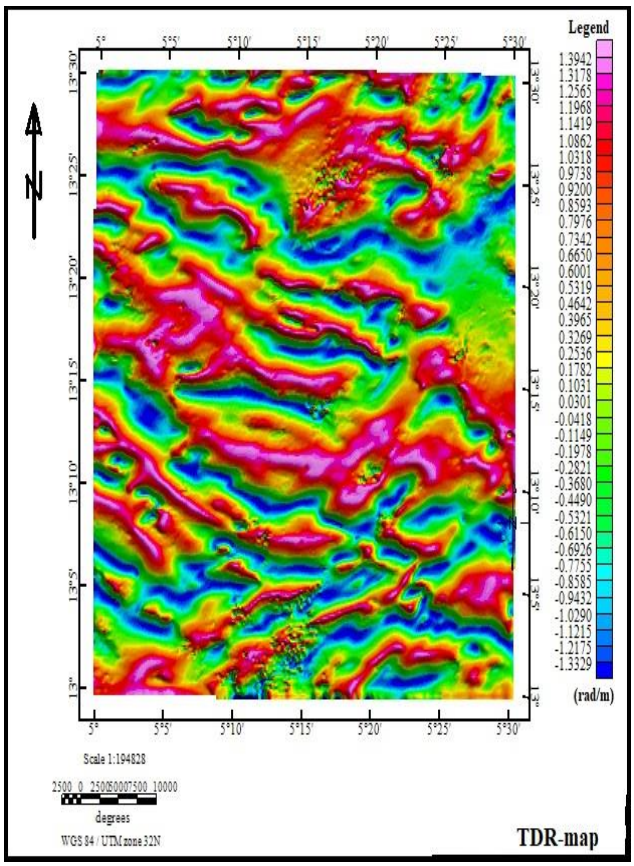

Fig. 7. Map of the total horizontal gradient of tilt angle

4.5 Source parameter imaging

The SPI approach calculates the depth parameter based on the analytical signal's local wave number. [26] asserted that the method utilized gradient derivatives to benefit from the relationship between the sources' distance and each site's local wave number (k) of the predicted field. The ability to view the depth in raster format and establish the actual thickness of each anomaly makes the SPI technique superior than spectral depth analysis. The SPI grid imaging map (Fig. 8) displays a

variety of colours illustrating the contrast between various magnetic susceptibilities within the analyzed area. In general, places with shallow magnetic bodies are represented by the red-pink colour, and those with deep magnetic bodies are shown by the blue-green colour. According to the SPI depth result, there are two main source depths: a shallow source depth of 251 m (for shallow magnetic bodies) and a deeper source depth of 2274 m (for deep lying magnetic bodies). This result also demonstrates that the research area's sedimentary thickness is greatest in the northeast, middle portion, and northwest of the region, with a shallow thickness in the southern part, which typically trends in a N-S direction. Therefore, subsequent exploration should concentrate on the region with the highest sedimentary thickness [29].

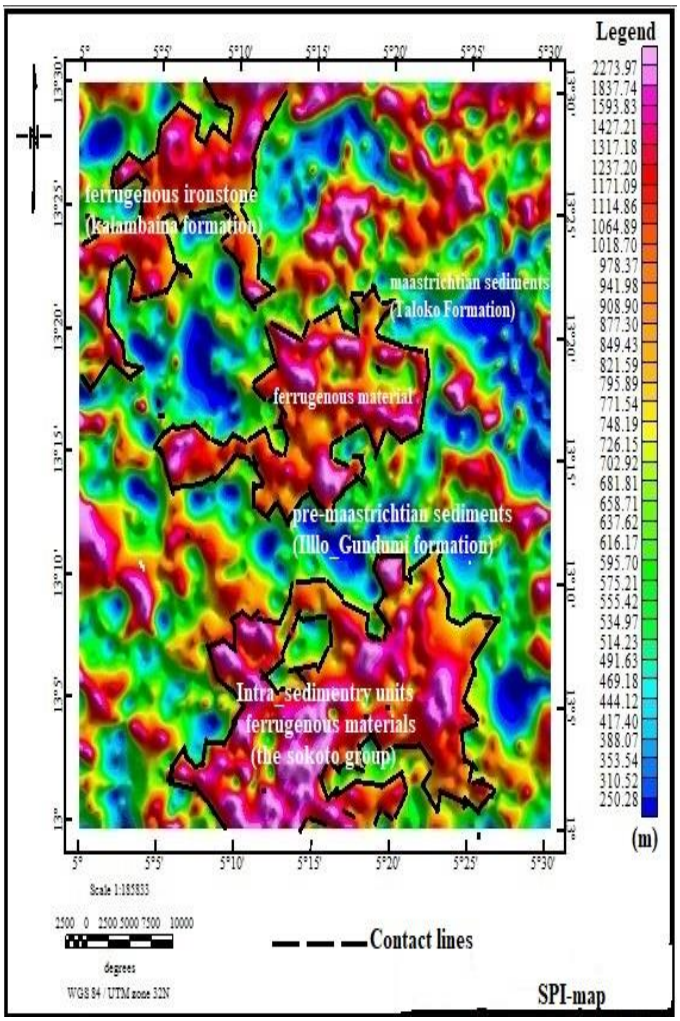

Fig. 8. Map of the Source parameter imaging (SPI), outlining the contact boundaries of intra-sedimentary unit of ferruginous materials of the Rima group

4.6 Analysis of Spectral depth

The magnetic anomaly for the survey region was separated into cell blocks (A-P), and the radially averaged power spectrum was produced in order to compute the depth utilizing the spectral approach for this study. A plot of the power spectrum against frequency (Fig. 9 (a,b)) gives an estimate of the depth to the magnetic source. The plot's low frequency component corresponds to deeper sources, while the plot's middle frequency and high frequency portions correspond, respectively, to shallow sources and noise. If the frequency unit is measured in radians per kilometer, the mean depth, Z, to the magnetic source is given by Z = —m/2; if measured in cycles per kilometer, Z = —m/(4*pi), where m is the slope.

According to the results of the spectral study, Block M has the thickest sedimentary layer (1.69 km), whereas Block D and Block E have the shallowest anomalies (0.39 km and 1.10 km, respectively) and the deepest sources (3.037 km), respectively (Table 1 and Fig. 10). Shallow anomalies have an average depth of 0.78 km, whereas deep-seated causes have a depth of 2.894 km (Table 1 & Fig. 10).

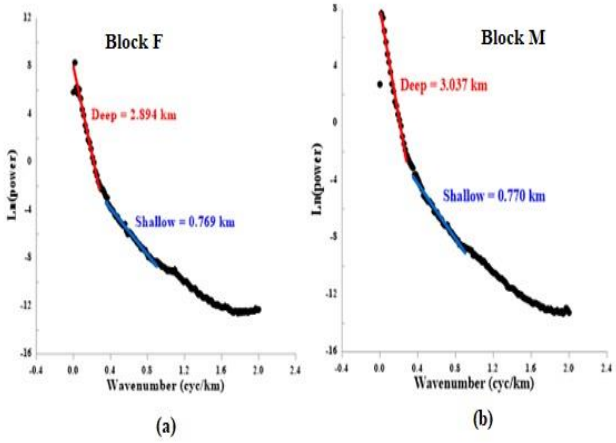

Fig. 9 (a-b). A visualization of a spectral block that was derived from an RTE anomaly map, illustrating the deep and shallow plate sources of depths

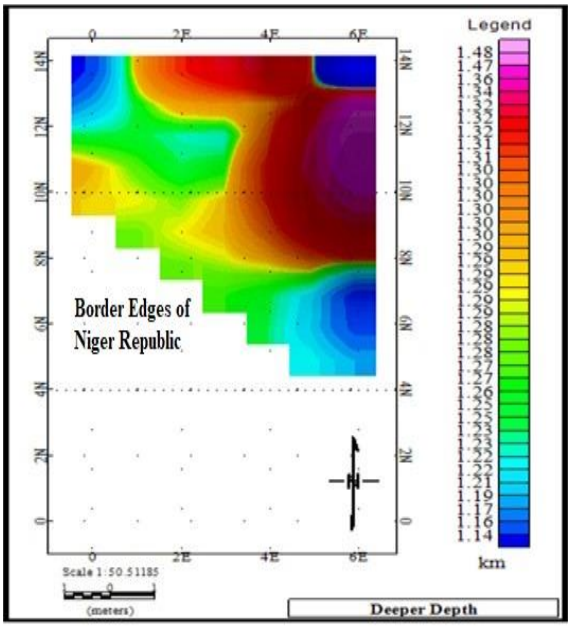

(a)

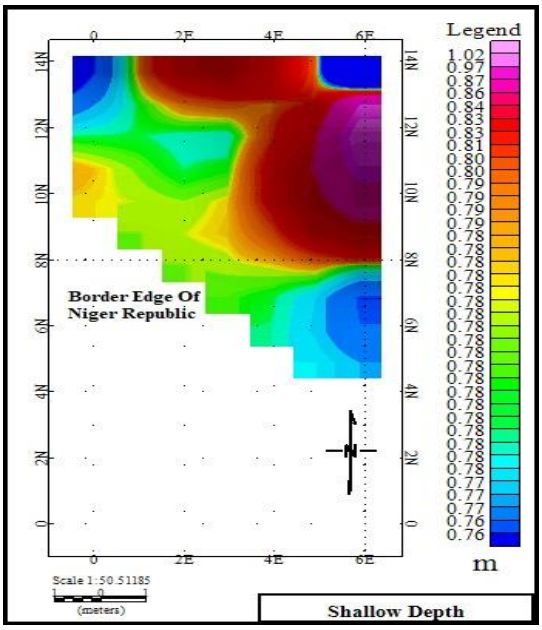

(b)

Fig. 10. 2D depth map obtained from the spectrum plots of **(a)** Deeper source **(b)** Shallow source

Table 1. Depth of information obtained from spectral plots over the study area.

Spectral blocks	Latitudes (N°)	(E°)	Depth (Km)	
			Deep	Shallow
A	13.400	5.099	0.99	1.27
B	13.400	5.241	0.95	1.11
C	13.393	5.391	0.63	1.22
D	13.393	5.533	0.39	1.28
E	13.285	5.099	0.53	1.34
F	13.285	5.241	0.77	2.89
G	13.282	5.391	0.48	1.38
H	13.281	5.531	0.73	1.11
I	13.155	5.099	0.84	1.34
J	13.156	5.241	0.77	1.10
K	13.152	5.391	1.30	1.62
L	13.152	5.533	0.83	1.41
M	13.150	5.534	0.77	3.04
N	12.969	5.241	0.96	1.22
O	12.967	5.101	0.61	1.34
P	12.970	5.531	0.88	1.22

5. CONCLUSION

Digital filtering tools such as total horizontal derivative of tilt angle, analytic signal, Spectral depth analysis, and Source parameter imaging were used to thoroughly analyze the HRAM data over the southern Taloka Formation and its surrounding areas in the Sokoto Basin, NW Nigeria. The following significant inferences can be made based on the use of the aforementioned tools:

a) Making use of HRAM data from the southern Taloka formation in NW Nigeria was found to be helpful in mapping and understanding the lithological structural properties related to mineralization potential in the area of study.

b) The analytic signal map we can shows that the amplitude was high (0.078 nT/m) over the edge of the magnetic structures in NW part of Kalambaina formation and southern part of the intra sedimentary unit (sokoto group) due to magnetic anomalies around these areas, which are associated with ferromagnetic properties that are more of Fe-bearing rocks. These high magnetic zones were consociated with iron stone, limestone, siltstone, hematite, magnetite and greenalite. The low magnetic zones with amplitude ranging from 0.009nT/m to 0.004nT/m are also delineated to be in NE part of Maastrichtian Sediment (Taloka formation) and eastern part pre-masstrichtian sediments of (illo and Gundumi formation) to western part of the masstrrichtian sediment of (Taloka formation). These regions of low amplitude are associated with sandstones, clays, shale's, when compared with geologic map. These regions exhibit the properties of diamagnetic minerals that usually have a weak negative magnetic anomaly within the sedimentary Basin.

c) The tilt of angle derivative and total horizontal tilt of and derivative maps reveals structures (faults, fractures and shear zones) that might host solid minerals in the northern, north-western and south-eastern part of the study area since minerals are structurally control. These structures trends NE-SW, NW-SE and E-W.

d) The thickness of the thickest sedimentary portion rarely exceeded 2 km, and other magnetic depth bodies are attributed to intrusive bodies, some boundaries within the sediments, other magnetic discontinuities, and shallow plates, according to the HRAM anomaly data that was presented through enhancement and depth filters like the horizontal derivative of tilt angle, analytic signal, spectral/wave number, and SPI.

e) Depths derived from spectral analysis and source parameter imagings are, respectively, 0.77 to 2.89 kilometers, and 0.251 to 2.270 kilometers, depending on the scale of parameter resolution. All of these depths provide values for terrain clearance, sediment thicknesses, and heights of intrusive within basement and sediments.

ACKNOWLEDGMENTS

The head of the applied geophysics department at the Federal University of Birnin Kebbi in Nigeria provided technical assistance, and the authors are appreciative for his words of support and encouragement.

REFERENCES

[1] C. A. Kogbe, "Geology of southeastern portion of the Iullemmeden Basin (Sokoto Basin)", Bull. Dept. Geology, Ahmadu Bello University, Zaria, Nigeria. Vol.2, pp. 42-64, 1979.

[2] N. G. Obaje, "Geology and Mineral Resources of Nigeria" [Online]. Available from: http://www.springerlink.com/index/10.1007/978-3-540-92685-6. 2009.

[3] P. Kearey, M. Brooks, and I, Hill. "An Introduction to Geophysical Exploration", 3rd edn, Oxford: Blackwell Publishing, USA: Iowa state university press.

[4] GETECH "Advanced Processing and Interpretation of Gravity and Magnetic Data, UK., 2007.

[5] A. Adamu, O. K. Likkason, A. S. Maigari, S. Ali, and E. A. Agada, "Subsurface Investigation of Geological Structures from Magnetic Method in Parts of Kangiwa Gwandu Formation, NW Nigeria", Six International Conference on Engineering Geophysics, (ICEG) Virtual, 25-28 October, 2021, United Arab Emirate University, Al-Ain, Abu-Dhabi, DOI: 10.1190/iceg2021-085.1. Pp. 336-341.

[6] W. Lowrie, "Fundamentals of Geophysics" (Second ed.). Newyork: Cambridge University Press. www.cambridge.org/isbn/9780521859028. pp.43–73, 2007.

[7] C. A. Kogbe, "Cretaceous and Tertiary of the Iullemmeden Basin in Nigeria (West Africa)", Cretaceous Research Vol. 2, pp. 129 – 186, 1981.

[8] J. D. Fairhead, "Advances in Gravity and Magnetic Processing and Interpretation", (EAGE Publications), 2015.

[9] O. K.. Likkason, G. P. Singh, and N. K. Samaila, "A study of the Middle Benue Trough (Nigeria). Based on Geological Application and Analysis of Spectra of Aeromagnetic Data-in Energy sources part, Recovery Utiliztion and Environmental Effects", Doi: 10.1080/15567036.2010.514588, 2013.

[10] W. M. Telford, L. P. Geldert, R. E. Sheriff, D. A. Keys, "Applied Geophysics, Cambridge University Press, Cambridge, London, Sydney, Pp. 323-342, 1976.

[11] O. K. Likkason, "Exploring and Using the Magnetic Methods – in Advanced Geosciences and Remote Sensing", Intechopen, https://dx.doi.org/10.5772/57163. 2014.

[12] W. J. Hinze, R. R. B. Von Frese, and A. H. Saad, "Gravity and magnetic exploration: Principles, practices, and applications", 2010.

[13] R. J. Blakely, "Potential Theory in Gravity and Magnetic Applications", Cambridge University Press, Cambridge, UK., pp.461, 1996.

[14] Geosoft Inc. "Defining and applying filters and inverse FFT in MAGMAP". Www.Geosoft.Com., pp.1–27, 2015.

[15] M. N. Nabighian, "The Analytic Signal of Two-Dimentional Magnetic Bodies with Polygonal Cross-section: Its Properties and Use for automated Anomaly Interpretation. Geophysics. Vol. 37, 1972.

[16] M. Mushayandebvu, P. van Drielz, A. Reid, and J. Fairhead. "Magnetic source parameters of two-dimensional structures using extended Euler deconvolution", Geophysics, Vol. 66, 814-823, 2001.

[17] P. S. Naidu, and M. P. Mathew, "Digital analysis of aeromagnetic maps: detection of a fault", J. Applied Geophysics Vol. 38, pp. 169-179, 1998.

[18] G. K. Anudu, R. A. Stephenson, and D. I. M. Macdonald, "Using high-resolution aeromagnetic data to recognise and map intra-sedimentary volcanic rocks and geological structures across the Cretaceous middle Benue Trough, Nigeria. Journal of African Earth Sciences. Vol. 99, pp.625–636, 2014.

[19] I N. MacLeod, K. Jones, and T. F. Dai, "3-D analytic signal in the interpretation of total magnetic field data at low magnetic latitudes", Exploration Geophysics. Vol. 24, pp. 679– 688, 1993.

[20] W. R. Roest, and M. Pilkington, "Identifying remanent magnetization effects in magnetic data", Geophysics. Vol. 58, pp.653–659, 1991.

[21] J. D. Fairhead, and C. S. Okereke, "A regional gravity study of the West African rift system in Nigeria and Cameroon and its tectonic interpretation", Tectonophysics, Vol. 143, pp. 141–159, 1988.

[22] J. D. Fairhead, A. Salem, L. Cascone, M. Hammill, S. Masterton, and E. Samson, "New developments of the magnetic tilt-depth method to improve structural mapping of sedimentary basins", Geophysical Prospecting. Vol. 59, pp.1072–1086, 2011.

[23] Geosoft Program (Oasis Montaj), "Geosoft Mapping and Application System Inc", Suit 500, Richmond St. West Toronto, ON Canada N5SIV6, 2007.

[24] A. Salem, S. Williams, J. D. Fairhead, D. Ravat, R. Smith, "Tilt-depth method: A simple depth estimation method using first-order magnetic derivatives", The Leading Edge, Vol. 26, pp. 1502–1505. https://doi.org/10.1190/1.2821934. 2007.

[25] S. A. Saada, "Edge Detectionand Depth Estimation from Magnetic Data of Wadi Arab, Eastern Desert-Egypt", IOSR Journal of Applied Geology and Geophysics Vol.3, pp.2321–990, 2015.

[26] J. B. Thurston, and R. S. Smith, "Automatic conversion of magnetic data to depth, dip, and susceptibility contrast using the SPI (TM) method", Geophysics. Vol. 62, pp. 807, 1997.

[27] A. Salem, R. Blakely, C. Green, D. Fairhead, and D. Ravat, "Estimation of depth to top of magnetic sources using the local-wavenumber approach in an area of shallow Moho and Curie depth — The Red Sea. Interpretation". Vol. 2, pp.1–8. 2014.

[28] Y. Li, Y. Yang, and T. Liu, "Derivative-based techniques for geological contact mapping from gravity data". Journal of Earth Science. Vol. 21, pp. 358–364, 2010.

[29] O. B. Nwosu, "Determination of Magnetic Basement Depth Over Parts of Middle Benue Trough By Source Parameter Imaging (SPI) Technique Using HRAM," Vol. 3, pp. 262–271, March, 2014.

[30] A. Spector, and F. S. Grant, "Statistical models for interpreting aeromagnetic data," Geophysics. Vol, pp.293–302, June, 1970.

[31] R. T. Shuey, D. K. Schellinger, A. C. Tripp, and L. B. Ali, " Curie depth determination from aeromagnetic spectra," Geophysical Journal of the Royal Astronomical Society. Vol. 50, pp.75–101. March, 1977.

[32] L. I. Nwankwo, and A. T. Shehu, "Evaluation of Curie-point depths, geothermal gradients and near-surface heat flow from high-resolution aeromagnetic (HRAM) data of the entire Sokoto Basin, Nigeria," Journal of Volcanology and Geothermal Research vol. 17, pp 45-62, September 2015. doi: 10.1016/j.jvolgeores.

[33] H. Zhang, Y. R. Marangoni, X. Hu , and R. Zuo, "A new reduction to the pole method at low latitudes via a nonlinear thresholding," Journal of Applied Geophysics. 111, pp.220–227, April 2014.